Environmental Science **Processes & Impacts**



PAPER



Cite this: Environ. Sci.: Processes Impacts, 2021, 23, 160

Fate of transition metals in PO₄-based in vitro assays: equilibrium modeling and macroscopic studies*

Brian. E. Reed, * Jayashree Yalamanchili, Jennie. B. Leach and Christopher, J. Hennigan (1)

Transition metals are thought to be among the most toxic components in atmospheric particulate matter (PM) due to their role in catalyzing reactive oxygen species (ROS) formation. We show that precipitation of the transition metals Fe(II), Fe(III), and Mn(II) are thermodynamically favored in phosphate-based assays used to measure the oxidative potential (OP) – a surrogate for toxicity – of PM. Fe and Mn precipitation is likely to occur at extremely low metal concentrations ($<0.5 \mu M$), levels that are imperceptible to the naked eye. The concentration of each metal (other than Cu) in aqueous PM filter extracts often exceeds the solubility limit in OP assays, indicating favorable thermodynamic conditions for precipitation. Macroscopic experimental results at higher metal concentrations (>100 µM) with visible precipitates provide quasi-validation of the thermodynamic modeling. Oxidation of Fe(III) to Fe(IIII) is likely to be rapid in all in vitro OP assays, transforming Fe to a much less soluble form. Fe precipitates are likely to increase the rate of precipitation of other metals and possibly induce co-precipitation. These results have direct relevance for all PO₄-based assays; the implications for studies of PM toxicity are discussed.

Received 21st September 2020 Accepted 19th December 2020

DOI: 10.1039/d0em00405g

rsc.li/espi

Environmental significance

In vitro assays are used to approximate the oxidative stress that results from particulate matter (PM) exposure by measuring oxidative potential (OP, a proxy for PM toxicity). While these assays have been used extensively to study organic compounds, they are also being used to determine the OP of transition metals. Several OP assays employ phosphate to buffer the system at pH = 7.4 for biological relevance. In this work, we show that oxidation and precipitation of many transition metals, including those present at high concentrations in atmospheric PM, occurs in this buffered phosphate matrix. This raises important questions about the use of such assays to assess PM toxicity.

Introduction

Particulate matter (PM) exerts numerous deleterious effects on human health, 1,2 which contributes significantly to the global burden of disease.^{3,4} There is strong evidence that PM induces oxidative stress, and this is hypothesized as a critical link between PM exposure and many adverse health outcomes.⁵⁻⁸ If true, this implies that the chemical species present in PM have different toxicities, since individual compounds have different reactivities and catalyze or form variable amounts of reactive oxygen species (ROS).

Acellular methods have been widely deployed to approximate the oxidative stress that may result from PM exposure through measurements of oxidative potential (OP). The general

Department of Chemical, Biochemical and Environmental Engineering, University of Maryland, Baltimore County, 1000 Hilltop Circle, Baltimore, Maryland, USA, 21250. E-mail: reedb@umbc.edu

† Electronic supplementary information (ESI) available. See DOI: 10.1039/d0em00405g

approach is to select a compound that reacts with cellular oxidants, and measure its time-dependent decay when exposed to PM extracts. The OP of the sample or matrix scales linearly with the blank-corrected reaction extent in a given time. Because oxidative stress is definitively linked to many disease outcomes, the acellular OP measurements are taken as a proxy for PM toxicity.9 A variety of OP assays have been developed, including dithiothreitol (DTT),10 ascorbic acid (AA),11 and glutathione.12

In order to mimic conditions within human lungs, most of the assays are run at 37 °C and pH = 7.4, often using a phosphate buffer to keep the pH constant. 10,11,13 However, under these conditions, precipitation, co-precipitation, complexation with PO₄, adsorption and oxidation of metals present in PM (and PM extracts) are thermodynamically possible. The catalytic properties of metals change drastically with phase (solid vs. aqueous), solids composition (e.g., Fe₂O₃(s) vs. Fe₃O₄(s)), and oxidation state.14,15 Fe, the transition metal present in ambient PM at the highest concentrations, 16,17 can form iron-oxides that have a well-known ability to adsorb other soluble metals. 18-20 These phenomena may contribute to some of the inconsistency in studies characterizing the health effects of specific PM components. DTT consumption rates for organic compounds are widely reported to be linear with the contaminant concentration but for metals the relationship is often reported to be a power law response – the DTT consumption rate levels off at high metal concentrations. Chemical and physical transformations of transition metals may represent a previously unidentified artifact associated with OP assays used as proxies for PM toxicity.

The purpose of this study is to characterize the behavior of several PM metals in PO_4 -based *in vitro* incubation fluids using MINEQL thermodynamic software²⁵ and quasi-validate modeling results using visual observations and metal fate experiments. Cu(II) and Mn(II) were chosen because of their high reactivity in acellular OP assays^{23,24,26} while Fe(II)/Fe(III) were chosen because they are often present in PM at concentrations an order of magnitude higher than other transition metals. ^{16,17} Equilibrium modeling results guide future experimental work on the fate of metals in PO_4 -based acellular incubation fluids and the effect of metal precipitation on ROS generation.

Materials and methods

Modeling approach

The behavior of the studied metals were assessed as a function of precipitate type, pH, [TOTPO₄], [TOTCO₃], partial pressure of $O_{2(g)}(P_{O_a})$ and iron-oxide concentration (for the adsorption of metals by iron oxide precipitate). Thermodynamic data (Tables S1-S4, ESI†) contained in MINEQL were supplemented with data from the NIST database as needed.27 Unless otherwise noted model runs were conducted at pH = 7.4, ionic strength (I) = 0.22 M, total TOTPO₄ = 0.1 M, TOTCO₃ = $1.4 \times 10^{-4} \text{ M}$ (closed system), and T = 37 °C. MINEQL corrects equilibrium constants for ionic strength and temperature using the Davies and Van't Hoff equations, respectively. An ionic strength of 0.22 M is based on the addition of 0.08 M of KH₂PO₄ and 0.02 M of KH₂PO₄ a common recipe for PO₄-based assays. The effect of TOTCO₃ on metal precipitation/complexation was studied by assuming that the phosphate buffer and other reagents had equilibrated with the atmosphere ($P_{\text{CO}_2} = 10^{-3.5} \text{ atm}$) at pH = 7.4 during DI water/ reagent storage, and then introduced to the assay incubation tubes (closed system with minimal headspace, T = 37 °C), resulting in $TOTCO_3 = 1.4 \times 10^{-4}$ M. For the effect of dissolved oxygen, we assumed conditions ranging from very low levels $(\log P_{\rm O_2} = -0.69 \text{ atm})$ to saturation $(\log P_{\rm O_2} = -50 \text{ atm})$. In Table S5,† modeling procedures for each task are presented based on the steps employed in MINEQL. The behavior of antioxidants (e.g., DTT) in the metal-PO₄ mixtures was not modeled because thermodynamic data (e.g., redox equilibria, stability constants) were not available. In addition, we acknowledge the uncertainty that arises with equilibrium modeling due to: (1) the inherent difference in reported constants, (2) assuming equilibrium conditions for systems that may not be at equilibrium and (3) applying constants determined under specific experimental conditions (metal concentration, temperature and ionic strength) to systems having different conditions.

Macroscopic experiments

Precipitation and oxidation experiments were conducted to help assess which solids would form in the phosphate buffer, thus quasi-validating the thermodynamic modeling. Stock solutions were prepared using reagent-grade metal salts stored in 2% nitric acid solutions. The metal concentrations in the stock solutions were quantified by ICP-MS (NexION 300D, PerkinElmer). Experiments were conducted at metal concentrations between 5 and 5000 µM in the presence of phosphate buffer (10^{-5} to 0.1 M) and in DI water. PO $_4$ solutions and DI water were oxygenated prior to use. Samples were prepared and placed in a thermomixer for 30 min at 37 °C and 400 rpm conditions used in the DTT assay. 10-12,23 Samples were allowed to settle for 10 min after which pictures were taken and a 30 mL aliquot was passed through a 0.45 µm filter. Aliquots were immediately (<5 min) analyzed for Cu(II), Mn(II), Fe(II), total Fe, and Fe(III) (by difference) using colorimetric methods (HACH, TOTFe: 8008; TOTFe(II): 8146; TOTFe(III) by difference; TOT-Cu(II): 8143; TOTMn(II): 8149).28 Interference from the high phosphate levels precluded the use of ICP-MS for metals analysis. Calibration curves were developed for a range of PO₄ concentrations and all curves were linear (Fig. S1, ESI†). Most of the macroscopic experiments were conducted in triplicate and all showed a very high degree of reproducibility. The standard deviations of the amount precipitated for each metal are as follows: Fe(III): 2.2%; Fe(II): 2.7%; Cu(II): 1.0%; Mn(II): 1.8 (Table S7, ESI†). In Fe(II) oxidation experiments the average standard deviation for Fe(II) and Fe(III) measurements were 0.5 and 2.8, respectively. Macroscopic visual experiments were conducted in the presence of DTT (100 µM) and the absence. DTT did not inhibit precipitation for any of the metals studied (Fig. S2-S5†).

Results and discussion

Precipitate type

Fe, Cu, and Mn can each form a number of precipitates. Our first goal was to identify the precipitates most likely to form and their corresponding solubility under conditions present in PO₄based acellular assays. Each precipitate was considered separately in MINEQL - other precipitates were prohibited. In Fig. 1, the metal solubility results (total concentration of all aqueous phase metal species) are presented for each precipitate type. All metals formed hydroxides, oxides or PO₄-based precipitates. Aqueous metal concentrations in PM oxidative potential studies typically range from 0.5 μ M to \sim 50 μ M 23,24,26 and all studied metals had at least one precipitate with a solubility lower than 5 μM. For subsequent modeling tasks we selected one PO₄-based (if one formed) and one non-PO₄ precipitate for each metal/ oxidation state. The chosen precipitates are represented by the cross-hatched bars in Fig. 1. For Fe(II) and Mn(II), only PO₄based precipitates were considered because the solubilities of the oxide/hydroxide precipitates were much higher than the concentration of these metals in PM extracts. Cu(I), Mn(III) and Mn(w) only form oxide type solids. For Mn(III), manganite (MnO(OH)(s)) was selected because iron is a component of bixbyite²⁹ and Mn(IV) only forms pyrolusite (MnO_{2(S)}). For Cu(II),

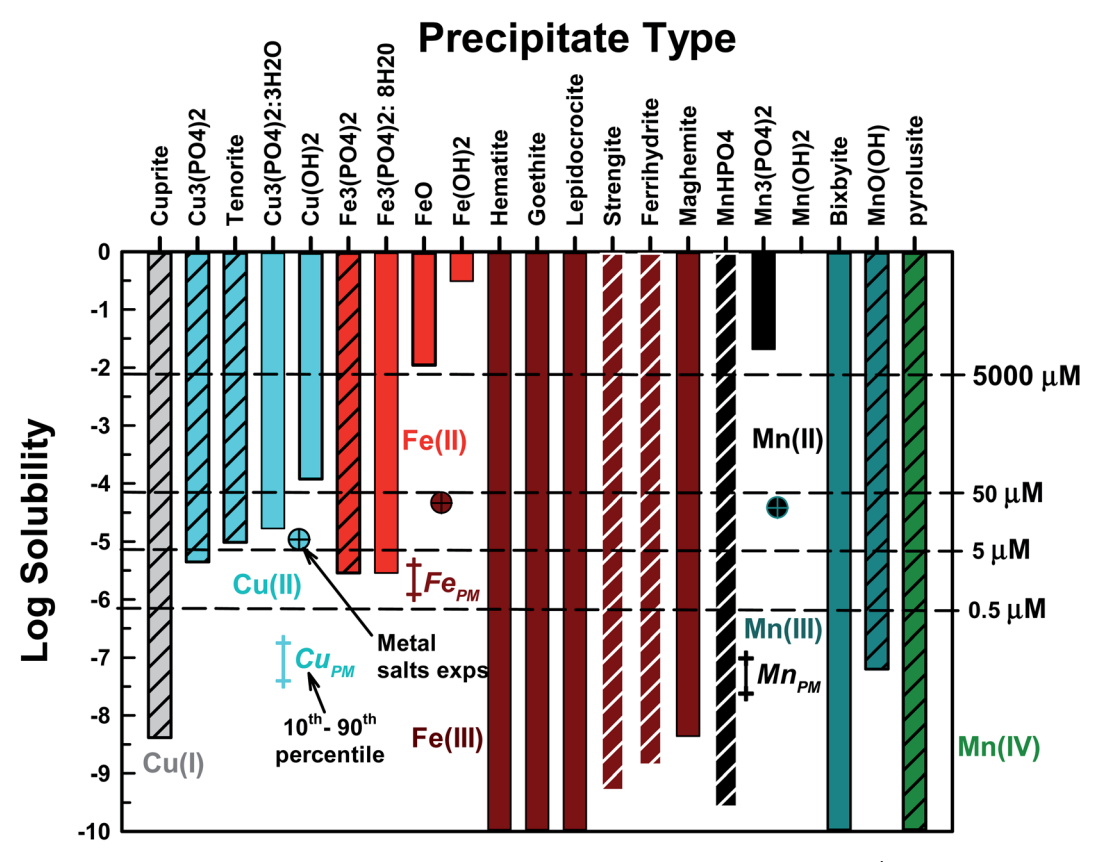


Fig. 1 Thermodynamic predictions of metal solubility at pH = 7.4, TOTPO₄ = 0.1 M, TOTCO₃ = 1.4 \times 10⁻⁴ M, I = 0.22 M and T = 37 °C. Crosshatched bars are solids that were selected for further study. Me_{PM} data represent the 10^{th} to 90^{th} percentile average of urban PM, in conditions of aqueous PM filter extracts. Single cross-hatched data points represent the highest metal concentrations used in metal salt experiments.

 $Cu_3(PO_4)_{2(s)}$ and tenorite $(CuO_{2(s)})$ were chosen because at 5 μM TOTCu a precipitate formed (the remaining Cu precipitates have solubilities >5 μM). Selecting which nonPO₄-based Fe(III) solid was most likely to form was more difficult because of the large number of potential precipitates. For reasons discussed in detail below, we chose strengite (FePO₄·2H₂O) and ferrihydrite $(Fe(OH)_{3(s)})$. Rather than use the terms "iron-oxide-like" or "iron-PO₄-like" (or "Mn/Cu-oxide-like" or "Mn/Cu-PO₄-like") to denote newly formed precipitates, we choose to use the crystalline name with the caveat that the precipitates are likely in the amorphous form. In addition, solubility products (K_{S0}) for amorphous solids are not readily available and we acknowledge that using K_{S0} for crystalline precipitates will result in a lower predicted solubility compared to the amorphous solids. For all metals, carbonate-based solids and complexes were not present. The behavior of Fe(II) and Fe(III) will be discussed together because Fe(II) is predicted to rapidly oxidize to Fe(III) under these conditions.

MINEQL runs were conducted with precipitation allowed and prevented - conditions that represent the two extreme possible behaviors in PO₄-based assays (Fig. S7†). For the runs where precipitation was allowed, the precipitates described above (hatched bars in Fig. 1) were included in the model runs allowing for the most thermodynamically favored solid to form. The dominant species predicted for all simulation conditions are given in Table S6.†

The Me_{PM} data in Fig. 1 represent the 10th to 90th percentile average annual metal concentrations measured for ten urban areas across the US17 determined using well-established PM filter sampling and extraction protocols (e.g., following the approach of Verma et al., 2014).30 Note Me_{PM} data represent total metal concentrations, i.e., there was no differentiation between metal oxidation states. The single cross-hatched data points represent some metal concentrations examined in studies where metals were added as salts, shown for reference.23,24,26 Total Fe_{PM} data averaged 2.3 µM and 10th to 90th percentile concentrations were 1.24 and 4.0 µM, respectively. The highest Fe(III) and Fe(II) concentrations used in metal salt studies were 47 and 10 µM, respectfully. As discussed above, any aqueous Fe(II) is likely to be rapidly oxidized to Fe(III), and all five Fe(III) compounds considered here have solubilities that are orders of magnitude lower than the range of concentrations in filter extracts from PM sampled in urban areas. This strongly suggests that aqueous Fe in PM extracts, even for samples that represent low atmospheric concentrations as well as those used in metal salt studies, will rapidly precipitate in PO₄-based assays. Cu_{PM} data averaged 0.06 µM while the 10th to 90th percentile concentrations were 0.04 and 0.18 µM, respectively. The highest Cu(II) concentrations used in metal salt studies was 11 μ M. Cu_{PM} is well below the solubility limit for all Cu(II)species considered; therefore, precipitation of aqueous Cu in PO₄-based assays of PM toxicity is not likely. However, Cu(II) precipitation could occur in metal salt experiments if TOTCu(II) > 4.47 μ M (solubility of Cu₃(PO₄)_{2(s)}). While Cu(i) is highly insoluble, the redox conditions in the OP assays are oxidizing due to the presence of dissolved oxygen, suggesting that reduction of Cu(II) to Cu(I) and subsequent precipitation is unlikely. However, if Cu was present as Cu(1), precipitation is possible if Cu(I) is not oxidized to Cu(II). Mn_{PM} data averaged 0.058 μM while the 10th to 90th percentile concentrations were 0.024 to 0.098 µM, respectively. The highest Mn(II) concentration from metal salt studies was 39 µM. If Mn exists as Mn(II) and is not oxidized, Mn(II) precipitation is not predicted to occur. However, if Mn is present as Mn(III) or Mn(IV), or if Mn(II) is oxidized, then precipitation of aqueous Mn in PO₄-based assays is thermodynamically favored.

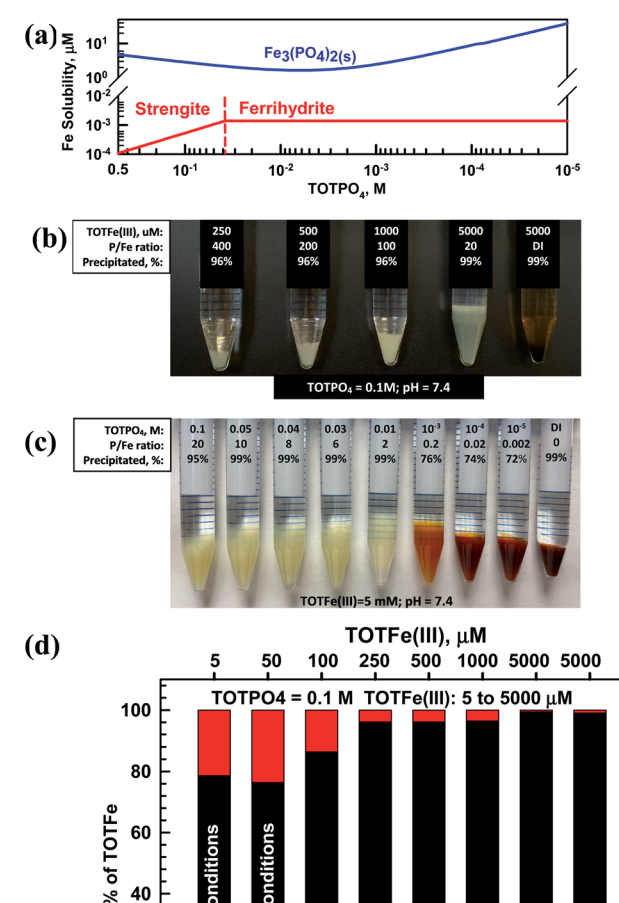
The effect of $K_{\rm so}$ (log $K_{\rm so} \pm 2$) on metal solubility was conducted for the selected precipitates to access the uncertainty in published values of K_{so} (Fig. S6†). Tenorite was most affected by the value of K_{so} , followed by $Cu_3(PO_4)_{2(s)}$, $Fe_3(PO_4)_{2(s)}$ and MnO(OH)(s). The remaining precipitates had solubilities well below 5 µM (the lowest metal concentration investigated).

In summary, precipitation of Fe and Mn is likely in PM filter extracts originating from urban areas and in metal salt studies. Cu(II) precipitation in PO₄-based assays is unlikely for PM extracts, but may occur in metal salt experiments if the total Cu(II) concentration exceeds 4.47 µM.

In the following sections, we discuss in detail the modeling results for each metal, focusing on the effects of pH, TOTPO₄, carbonate, and dissolved O₂. We present the macroscopic experimental results, including the visual presence/absence of precipitates and chemical analysis of dissolved metals. We acknowledge that the high metal concentrations used to visually observe precipitation do not represent metal concentrations in PM extracts unless samples were taken from heavily polluted areas or for extended periods of time. However, detection of precipitates at concentrations typical of PM extracts is challenged by the extremely low mass present. For example, 15 mL of Hi-Vol filter extract following the procedure of Verma et al.³⁰ contains approximately $\sim 2-8 \times 10^{-8}$ g of Mn (range representing urban concentrations in the US).16 Creative experimental approaches combined with advanced analytical techniques are required to physically detect precipitates at such low levels: this is the topic of ongoing work by our group. Therefore, we believe that the macroscopic experimental results are useful in understanding what can occur thermodynamically in PO₄-based assays in regards to precipitation, oxidation and changing assay conditions (e.g., effect of TOTPO₄).

Iron

Fe(II) formed Fe₃(PO₄)_{2(s)} and Fe(III) formed strengite or ferrihydrite depending on the magnitude of TOTPO₄ (Fig. 2a). Based on visual observations and the aqueous phase Fe(III) analysis, we are confident that strengite formed at higher TOTPO₄/TOTFe ratios (Fig. 2). Hsu (1982)31 reported that phosphate induces nearly immediate formation of a fluffy "whitish" precipitate, with \sim 98% of the Fe($\rm III$) in the precipitate at equilibrium. In



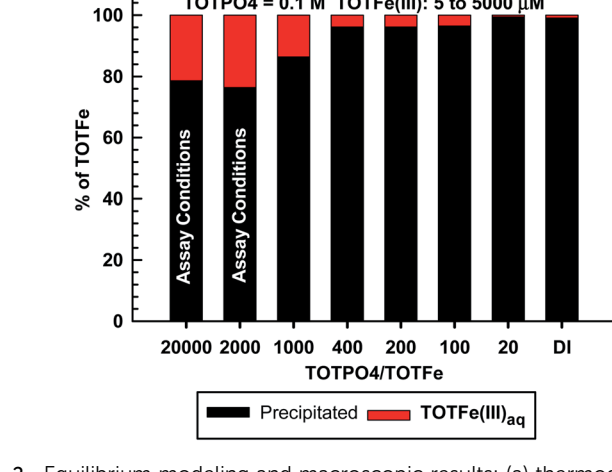


Fig. 2 Equilibrium modeling and macroscopic results: (a) thermodynamic predictions of Fe(III) and Fe(III) solubility as function of TOTPO₄; (b) macroscopic experimental results, including visual observations at $TOTPO_4 = 0.1 M$, with varying TOTFe(III); (c) macroscopic experimental results, with visual observations at TOTFe(III) = 5 mM, varying TOTPO₄ and (d) precipitation results for varying TOTFe(III), TOTPO₄ = 0.1 M. Note, in (b), (c), and (d) the percent of Fe precipitated is based upon chemical analysis.

a similar aqueous matrix, Senn et al. (2015)32 reported amorphous FePO_{4(s)} formation, which appeared beige in color. Senn et al. (2015)32 also observed shifting precipitate identity as a function of the TOTPO₄/TOTFe molar ratio: the Fe(III) suspension changed from "whitish" to an "orange" or "brownish" as TOTPO4/TOTFe decreased, indicating the formation of lepidocrocite (orange) or ferrihydrite (brown). We observed similar behavior in our experiments (Fig. 2b) - the type of solid clearly changed from beige (FePO_{4(s)}) to orange-brown between 0.01 and 0.001 M TOTPO₄ (initial Fe constant at 5 mM). When lepidocrocite and strengite are both allowed to form in MINEQL, 100% of the Fe(III) exists as lepidocrocite

(Fig. S8†), which does not match what we observed visually. Ferrihydrite and maghemite form at TOTPO₄ less than 0.037 M and 0.011 M, respectively. While maghemite formation matched the visual pattern better than ferrihydrite (Fig. S9†), we selected ferrihydrite because Singh *et al.* (2010)³³ reported that the precipitation of ferrihydrite is favored when hydrolysis occurs rapidly and ferrihydrite formation in the presence of PO₄ was reported by Senn *et al.* (2015).³²

At 0.1 M TOTPO₄/pH = 7.4 (conditions used in most PO₄-based acellular assays) precipitation of Fe(III) was observed visually over a wide range of TOTFe(III) (Fig. 2c). While we did not observe visible solid formation at low TOTFe(III) (a 10 mL solution of 50 μ M Fe contains only 2.8 \times 10⁻⁵ g of total Fe), precipitation was confirmed based on chemical analysis of filtered samples (Fig. 2d). Note, we confirmed that neither PO₄ nor DTT interfere with the Fe measurements. At 5 and 50 μ M TOTFe(III), about 80% of added Fe(III) precipitated, while 86–99% of Fe precipitated at higher TOTFe(III). Decreased precipitation at lower TOTFe(III) could be due to the presence of small strengite-type particles that escape filtration.³⁴ The remaining aqueous Fe(III) exists as Fe(OH)₂⁺ and Fe(OH)_{3(aq)} (Table S6†).

Fe(III) (as well as Fe(II), Cu(II) and Mn(II)) precipitation occurred experimentally at all TOTFe(III)-TOTPO₄ combinations within the 30 min duration of acellular assays. Precipitation is a two-step process of nucleation and crystal growth, with nucleation typically the rate-limiting step.³⁵ Nucleation can be considered homogenous (slow, random particle growth) and heterogeneous (fast, nucleation occurs on existing surfaces). To date, there have been no kinetic studies of FePO_{4(s)} growth under PO₄-based acellular conditions. However, Senn et al.32 and Madsen and Koch³⁴ investigated the formation of FePO_{4(s)} following the oxidation of Fe(II) to Fe(III). Senn et al. 32 conducted macroscopic studies and reported that within 6 min, a beige "Fe(III)-phosphate precipitate" formed after Fe(II) addition. At TOTPO₄/TOTFe <0.52, the suspension color changed from initially beige to orange over 240 min indicating that the formation of FePO_{4(s)} occurred first, followed by FePO_{4(s)} dissolution and then the formation of Fe(III)-oxide precipitate. While we did not observe this time-dependent transition, we did observe the apparent shift from Fe(III)-phosphate precipitate to Fe(III)-oxide precipitate at a similar P/Fe ratio (between 0.2-2 in our work).

It is highly likely that Fe(III)-oxide solid would form in acellular assays at lower TOTPO₄, suggesting that decreasing the phosphate buffer concentration would not prevent Fe(III) precipitation. Grundl and Delwiche³⁶ reported that ferric iron precipitation in the absence of phosphate was first order with respect to Fe(OH)_{3(aq)}: dFe(III)/d $t = -k[\text{Fe}(OH)_{3(aq)}]$. The precipitation rate decreased with increasing TOTFe(III) concentration (half-lives: 5 min and 15 min at TOTFe(III) = 500 and 1000 µM, respectively) due to the poisoning of the surface by Fe³⁺ and to a lesser extent by Fe(OH)²⁺. Grundl and Delwiche's work was conducted at pH 2.5–3 where Fe³⁺/Fe(OH)²⁺ are dominant, while at pH = 7.4 Fe³⁺/Fe(OH)²⁺ are essentially nonexistent. As with the other metals, our goal with this work is to characterize the predicted metal phase state and speciation in the PO₄ matrix. Connecting the formation of metal-complexes and precipitates

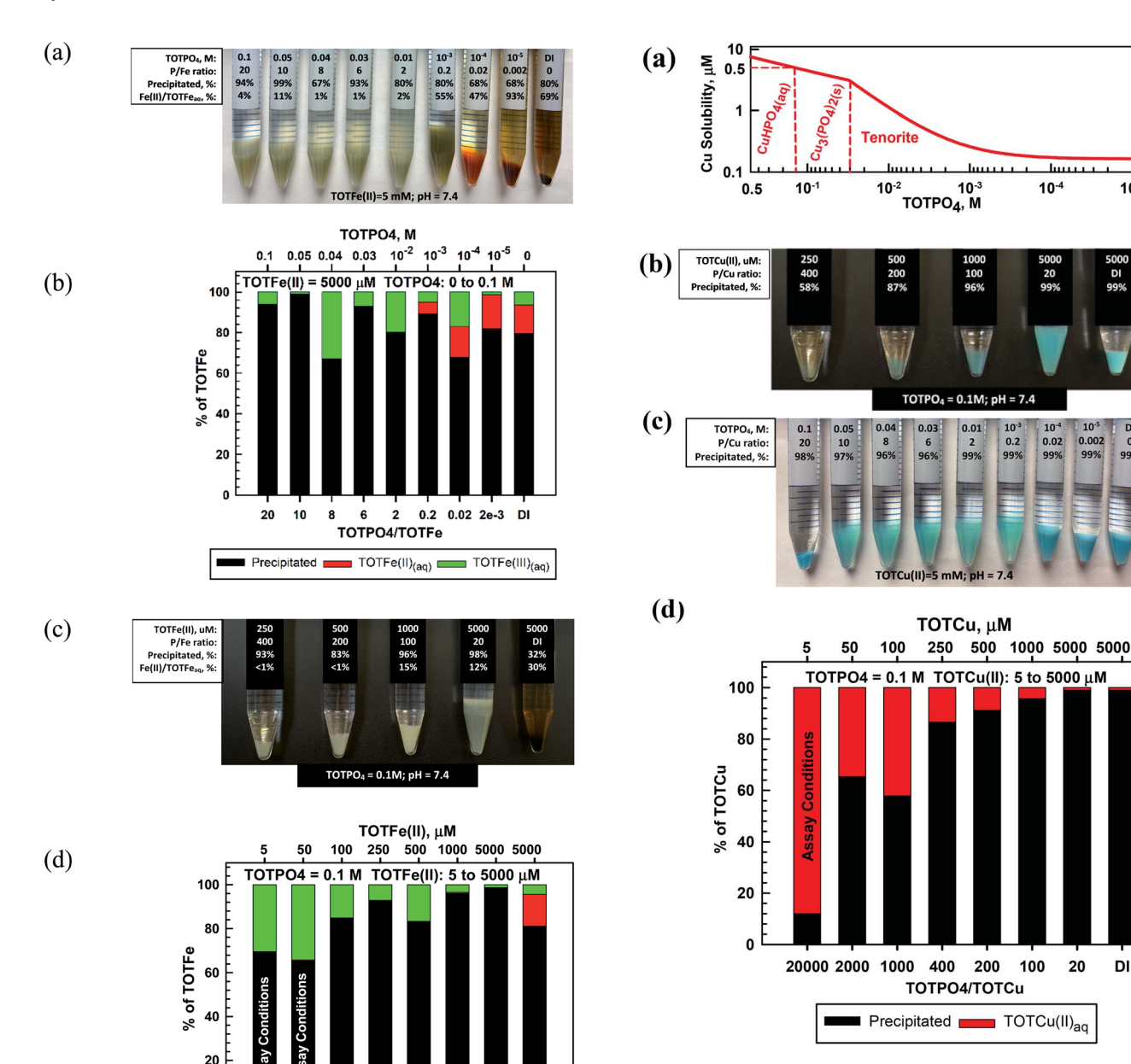
with the generation of ROS or the response of OP assays is beyond the scope of this study, but warrants attention. Metals can catalyze ROS formation in solid or aqueous form³⁷ therefore, it is likely that the formation of precipitates could also affect the DTT consumption rate.

The effect of $[O_{2(aq)}]$ on metal oxidation was investigated by varying the O_2 partial pressure from 0.21 to essentially zero (at 25 °C and $P_{O_2}=0.21$ atm, $[O_{2(g)}]\approx 275~\mu\text{M}$, 8.9 mg L $^{-1}$). Fe(II) is oxidized to Fe(III) at very low $[O_2]$ concentrations (Fig. S10†). Fe(II) and Fe(III) either form Fe₃(PO₄)_{2(s)} or strengite, respectively, depending on the P_{O_2} level. Sung and Morgan³⁸ summarized results from multiple studies on the kinetics of Fe(II) to Fe(III) oxidation in the natural environment. Half-lives ranged from \sim 16–47 min at pH levels between 6.3–6.52 and \sim 3.3–5.5 min at pH = 8.0. Madsen and Koch³⁴ reported that Fe(II) was oxidized in water with very low dissolved oxygen (DO) concentrations (H₂O purged with N_{2(g)}) and that iron phosphate solid catalyzed Fe(II) oxidation. These results indicate the likely rapid transformation of Fe(II) to Fe(III) during any *in vitro* measures of PM toxicity with phosphate in the assay matrix.

In our experiments, Fe(II) formed a whitish precipitated at $TOTPO_4 \ge 0.01$ M, transitioned to a grayish-white precipitate at $TOTPO_4 = 10^{-3}$ M, and then to an orange/brown precipitate at $TOTPO_4 \le 10^{-4} \text{ M (Fig. 3a)}$. For $TOTPO_4/TOTFe(II)$ combinations in which a whitish precipitate was observed, it is not possible to say if Fe₃(PO₄)_{2(s)} or strengite formed. However, when the orange/brown precipitates were present, it is clear that Fe(II) was oxidized to Fe(III) with subsequent Fe(III)-oxide solid formation. $FeO_{(s)}$ or $Fe(OH)_{2(s)}$ solid formation was not possible given their very high solubilities (FeO_{2(s)} – 0.011 M; Fe(OH)_{2(s)} – 0.31 M, Fig. 1). Fe(II) oxidation to Fe(III) is further demonstrated in the Fe(II)-DI water experiments, where ferrihydrite formed following Fe(II) oxidation to Fe(III). Chemical analysis of filtered samples also reinforces this observation – at TOTPO₄/TOTFe(II) \leq 0.2 and in DI water there was a mixture of Fe(II)/Fe(III) in the aqueous phase.

For $TOTPO_4 = 0.1 M$ a whitish precipitate formed at TOT-Fe(II) = 250 to 5000 μ M (Fig. 3c). At 5 and 50 μ M TOTFe(II) there was no visual precipitation but 70% and 65% of the total iron precipitated as either Fe₃(PO₄)_{2(s)} or strengite. At the lower TOTFe(II) there was significant oxidation of Fe(II) to Fe(III) based on analysis of filtered samples (Fig. 3d). Under similar conditions for TOTFe(III) = 5 to 100 μ M there was slighly more precipitation of Fe(III) but still a significant amount of Fe(III) in solution relative to higher TOTFe(III) concentrations (Fig. 2d). It is possible that the combination of Fe(III) oxidation to Fe(III) and Fe(III) precipitation to strengite were subject to slower kinetics than that observed at higher iron concentrations. Under PO₄based *in vitro* assay conditions (indicated in Fig. 3d) Fe(II) was oxidized and there was precipitation of either $Fe_3(PO_4)_{2(s)}$ or strengite (or both). Oxidation of Fe(II) to Fe(III) is highly likely to occur, though the identity of the specific solids is based upon specific conditions within the assay and we can speculate that these transformations will likely affect the generation of ROS in PO₄-based assays.

10-5



 Precipitated ■ TOTFe(II)_(aq) ■■■ TOTFe(III)_(aq) Fig. 3 Fe(II) macroscopic results: (a) visual observations at TOTFe(II) =upon chemical analysis. 5 mM, varying TOTPO₄; (b) precipitation/oxidation results at TOTFe(II) = 5 mM, varying TOTPO₄; (c) visual observations at TOTPO₄ = 0.1 M, varying TOTFe(II) and (d) and precipitation/oxidation results at TOTPO₄ = 0.1 M, varying TOTFe(II). Note all results in figures are based on

TOTPO4/TOTFe

100 20 DI

Copper

chemical analyses.

At pH = 7.4 Cu(II) exists predominantly as CuHPO_{4(aq)} (Fig. 4a and Table S7†). At slightly higher pH (>7.6), tenorite is predicted to form over $Cu_3(PO_4)_{2(s)}$ (Fig. S7†). For $TOTCu(II) \le 250 \mu M$ at $TOTPO_4 = 0.1 \text{ M/pH} = 7.4 \text{ there was no visible precipitate}$ formation (Fig. 4b); however, the aqueous Cu measurements

20000 2000 1000 400 200

Fig. 4 Cu(II) equilibrium modeling and macroscopic results: (a) thermodynamic predictions of Cu(II) solubility as function of TOTPO₄; (b) macroscopic experimental results, including visual observations at $TOTPO_4 = 0.1 M$, varying TOTCu(II); (c) macroscopic experimental results, including visual observations at TOTCu(μ) = 5000 μ M, varying $TOTPO_4$ and (d) precipitation results for varying TOTCu(II), $TOTPO_4 =$ 0.1 M. Note, in (b), (c), and (d) the percent of Cu precipitated is based

20

DI

indicate that precipitation did occur (Fig. 4d). At $TOTPO_4 \ge$ 0.14 M all Cu(II) exists as CuHPO_{4(aq)}; for TOTPO₄ between 0.14 and 0.03 M Cu₃(PO₄)_{2(s)} forms, while tenorite forms below 0.03 M TOTPO₄ (Fig. 4a). Matching visual observations to equilibrium modeling results is more difficult with Cu(II) because there were no changes in precipitate appearance (the deeper blue precipitates could be due to density differences of the settled solids). Cu(II) precipitation occurred experimentally at all TOTCu(II)-TOTPO4 combinations within the 30 min duration of in vitro assays. For all macroscopic experiments at $TOTPO_4=0.1~M/pH=7.4$, the measured $TOTCu_{(aq)}$ was always greater than the predicted $Cu(\pi)$ solubility (4.47 $\mu M)$. $Cu(\tau)$ in the acellular assay matrices would exist as aqueous $Cu(\tau)$ or $CuO_{2(s)}$ (Fig. S10†) or be oxidized to $Cu(\pi)$. It is interesting to note that $Cu(\pi)$ is reported to be the most active of the transition metals in generating ROS, 23 which could in part be due to its high solubility.

Manganese

Mn proved to be the most complicated of the metals studied because of its multiple oxidation states and precipitates. At $TOTPO_4 = 0.1 \text{ M/pH} = 7.4 \text{ Mn(II)}$ exists as MnHPO_{4(aq)} (95%; no precipitation, Table S7†) or MnHPO_{4(s)} (Fig. 5a). Mn(III) exists as Mn³⁺ or MnO(OH)_(s) (Table S7†). Mn(IV), a highly insoluble species (MnO_{2(s)} solubility = 2.3×10^{-13} M), does not form complexes with OH^- or PO_4 . At $TOTMn(II) \ge 500 \mu M$ and $TOTPO_4 = 0.1 \text{ M}$ a whitish precipitate formed (Fig. 5b) while at lower TOTMn(II) precipitation was demonstrated by measuring the Mn concentration in filtered samples (Fig. 5d). When precipitation was studied as a function of TOTPO₄, a whitish precipitate formed at $TOTPO_4 \ge 0.01 \text{ M}$ and a brownish/black precipitate at $TOTPO_4 \le 10^{-3}$ M (Fig. 5c). If we assume the whitish precipitate is MnHPO_{4(s)} then clearly a different solid formed at lower TOTPO₄. If MnHPO_{4(s)} formation does not occur, the remaining two Mn(II) precipitate solubilities $Mn_3(PO_4)_{2(s)}$ (0.02 M) and $Mn(OH)_{2(s)}$ (2.07 M) (Fig. 1) are far higher than what we measured.

Redox transformations of dissolved Mn are likely in PO₄based matrices, though the speciation of Mn is uncertain. Mn(II) can be oxidized to Mn(III) or Mn(IV) under lower DO concentrations with the subsequent formation of MnO(OH)(s) or MnO_{2(s)} (Fig. S10†). Stumm and Morgan³⁵ reported an Fe(II)-type oxidation relationship for Mn(II) to Mn(IV): $d[Mn^{2+}]/$ $dt = -k[OH^{-}]P_{O_{a}}[Mn^{2+}]$ with the Mn(II) oxidation rate very low at pH < 9. The oxidation rate may be higher in PO₄-based assays due to the higher temperature and higher [O₂] (assuming reagents are in equilibrium with the atmosphere). However, the formation of MnHPO_{4(aq)} complexes could slow the Mn(II) oxidation rate. Faust and Aly39 reported that Mn(II) oxidization is catalyzed by $MnO_{2(s)}$ and it is possible that $MnHPO_{4(s)}$ may catalyze the $Mn(II) \rightarrow Mn(IV)$ reaction but there are no literature results to confirm this mechanism. A more likely scenario is that Mn(II) is oxidized to Mn(III) with the formation of $MnO(OH)_{(s)}$ – at lower TOTPO4 we observe that the formation of the brown/blackish precipitate occurs experimentally at $TOTPO_4 \approx 10^{-3} \text{ M}$ (Fig. 5b) and $MnO(OH)_{(s)}$ is predicted to form at $TOTPO_4 = 5 \times 10^{-4}$ M (dotted blue line in Fig. 5a).

Adsorption by ferric iron precipitates

Adsorption of metals by iron oxides is a well-known phenomenon. In this task we investigated the adsorption of $Cu(\pi)$ and $Mn(\pi)$ onto hydrous ferric oxide (HFO) using the modeling approach of Dzombak and Morel. Fe(π) only forms ferrihydrite at TOTPO₄ < 0.037 M (Fig. 2a), thus HFO adsorption modeling is only applicable at phosphate

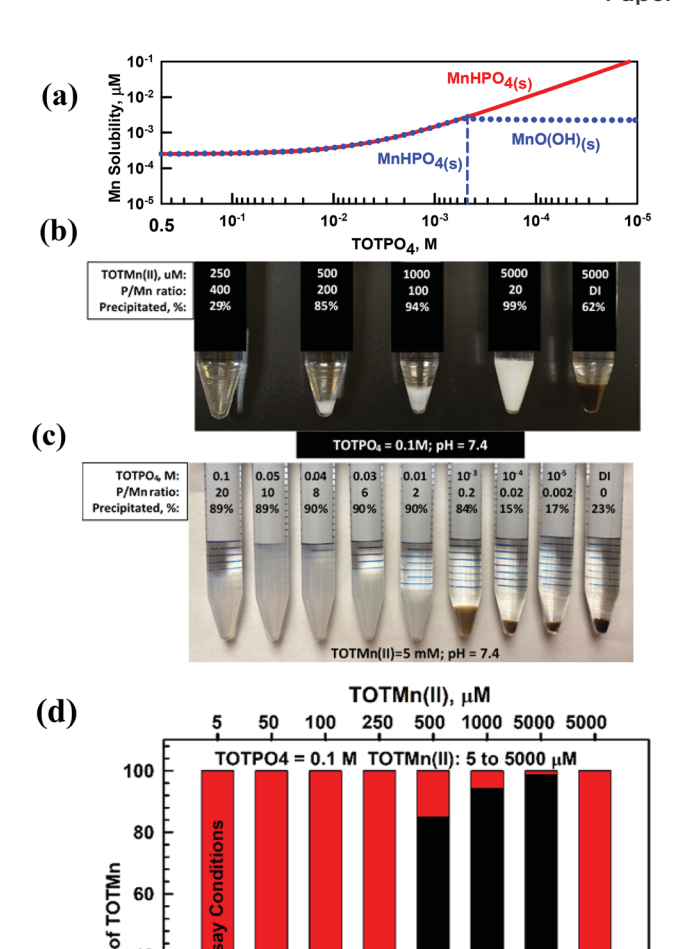


Fig. 5 Mn(II) equilibrium modeling and macroscopic results: (a) thermodynamic predictions of Mn(II) solubility as function of TOTPO4; (b) macroscopic experimental results, including visual observations at TOTPO4 = 0.1 M, varying TOTMn(II); (c) macroscopic experimental results, including visual observations at TOTPO4 and (d) precipitation results varying TOTMn(III), TOTPO4 = 0.1 M. Note, in (b), (c), and (d) the percent of Mn precipitated is based upon chemical analysis.

20

0

concentrations much lower than what are currently used in OP assays. At 50 μM Fe(III) (all of which was assumed to form HFO) there was minimal adsorption of Cu(II) and Mn(II) (Fig. S11†). Senn $et~al.^{32}$ reported that freshly formed FePO4(s) is capable of adsorbing metals, although there is no experimental data available to quantify FePO4(s) adsorption capacity. Iron oxide can adsorb orthophosphate40 and it is possible that FePO4(s) will also adsorb PO4. Given the high TOTPO4 used in OP assays we believe that PO4 will outcompete PM metals for adsorption sites and thus metal adsorption is likely of minimal concern.

Conclusions

Overall, the processes we report likely have profound importance for *in vitro* assays of PM toxicity. The results also inform prior studies of transition metal toxicity. Charrier *et al.*²³ and Fujitani *et al.*²⁴ reported DTT consumption rate series as:

$$Cu(\Pi) > Mn(\Pi) \gg Fe(\Pi) \sim Fe(\Pi)^{23}$$

 $Ni(\Pi) > Cu(\Pi) > Mn(\Pi) > Fe(\Pi)^{24}$

It is likely that Fe(III) and Fe(II), either added as a reagent or through collected PM, will precipitate in PO₄-based assays: Fe(III) precipitates as strengite and Fe(II) precipitates as $Fe_{3}(PO_{4})_{2(s)}.$ $Fe({\scriptstyle II})$ is readily oxidized to $Fe({\scriptstyle III})$ with subsequent precipitation of Fe(III). Mn(II) precipitates as MnPO_{4(s)} but the precipitation rate appears to be slow at Mn(II) concentrations present in PM extracts (<5 µM), a possible reason for the high ROS generation potential of $Mn(\pi)$. $Mn(\pi)$ oxidation to $Mn(\pi)$ is slow at pH < 9 so a more likely scenario is that Mn(II) is oxidized to Mn(III) with subsequent formation of MnO(OH)(s). It is notable that Cu is - by far - the most active metal in catalyzing DTT reaction.24 The ascorbic acid assay is also highly sensitive to Cu.11,41 If these measurements are surrogates for ROS generation in human lungs, then this implies that Cu possesses an enhanced toxicity compared to other metals present in PM.42 However, toxicological⁴³ and epidemiological studies^{44,45} generally do not support this assessment. This apparent disconnect is possibly due to its high solubility (~90% solubility at pH = 7.4, TOTPO₄ = 0.1 M, TOTCu(II) = 5 μ M).

Metal precipitation is highly likely in most assay matrices due to the high TOTPO $_4$ (\sim 0.1–0.5 M) and near-neutral pH (7.4) used to mimic biological systems. Decreasing TOTPO $_4$ in acellular assays (while still maintaining pH = 7.4) shifts the precipitate identity to favor the formation of oxide/hydroxide solids, while still allowing oxidation of Fe(II) and Mn(II). When actual PM material is evaluated in PO $_4$ -based assays, multiple metals will be present increasing the likelihood of coprecipitation and increased precipitation rates (e.g., Fe(III) readily precipitates and then is a source of nucleation sites for other metal precipitates).

On the one hand, this behavior is unsurprising since a defining characteristic of metals is their pH-dependent solubility and their known complexation chemistry with PO₄. However, this phenomenon has not been reported previously, likely because precipitate formation occurs even at low concentrations where solids are most likely colloidal in size and imperceptible to the human eye. Factors such as PM sample matrix, metal concentrations, and metal oxidation state can produce variability in metal precipitation (both rate and amount formed) suggesting that the process we report is quite variable within and between assays. Future studies should extend our results to include thermodynamic and experimental characterization of other PM metals, *e.g.*, V and Ni, in PO₄-based matrices.

The current study informs the fate and transformation of metals in OP assays that achieve pH control (typically pH = 7.4) using phosphate buffers. These include DTT, glutathione, and ascorbic acid. Our results likely extend to simulated (or surrogate) lung fluid (SLF), an acellular medium used to represent conditions in the human respiratory tract. The behavior and fate of metals in cellular assays is unknown, due to interactions between metals and cell culture media, especially organic molecules likely to form complexes with metals (e.g., proteins).

It is important to note that the effects of this phenomenon on assay response (*e.g.*, ROS generation or antioxidant depletion) are beyond the scope of the present study and have not been characterized. Metals in solid and aqueous form can induce ROS formation, ^{15,37} but it is likely that these would elicit quite different responses due to their different chemical forms and the surface effects associated with precipitates. For example the presence of antioxidants could facilitate rapid redox cycling of $Fe(\pi)/Fe(\pi)$, $Mn(\pi)/Mn(\pi)/Mn(\pi)$, *etc.* Additionally, the formation of precipitates could affect the formation of hydroxyl radicals, superoxide and H_2O_2 . We recommend that the effects of metal precipitation on ROS formation and differences in assay response to different chemical forms of each metal represent urgent research needs in understanding the health effects of PM and toxicity of individual PM constituents.

Data availability

All model inputs and outputs have been published, and are freely available at http://hdl.handle.net/11603/18201.

Conflicts of interest

The authors declare no competing financial interest.

Acknowledgements

This work was funded by the National Science Foundation through award #1802474. We acknowledge Bill Schecher, Chief Programmer, MINEQL, for technical assistance with MINEQL, and Aidan Mucci and Carlos Castillo Lara: Undergraduate Research Assistants, UMBC Department of Chemical, Biochemical and Environmental Engineering for assistance with laboratory assays.

References

- 1 C. Davidson, R. Phalen and P. Solomon, Airborne Particulate Matter And Human Health: A Review, *Aerosol Sci. Technol.*, 2005, 39(8), 737–749.
- 2 C. Pope and D. Dockery, Health Effects of Fine Particulate Air Pollution: Lines That Connect, *J. Air Waste Manage. Assoc.*, 2006, 56(6), 709–742.
- 3 Institute, H.E., Health Effects Institute, *State of Global Air*, 2019.
- 4 C. Liu, R. Chen, F. Sera, A. Vicedo-Cabrera, Y. Guo, S. Tong, M. Coelho, P. Saldiva, E. Lavigne, P. Matus, N. Valdes Ortega, S. Osorio Garcia, M. Pascal, M. Stafoggia, M. Scortichini,

- M. Hashizume, Y. Honda, M. Hurtado-Díaz, J. Cruz, B. Nunes, J. Teixeira, H. Kim, A. Tobias, C. Íñiguez, B. Forsberg, C. Åström, M. Ragettli, Y. Guo, B. Chen, M. Bell, C. Wright, N. Scovronick, R. Garland, A. Milojevic, J. Kyselý, A. Urban, H. Orru, E. Indermitte, J. Jaakkola, N. Ryti, K. Katsouyanni, A. Analitis, A. Zanobetti, J. Schwartz, J. Chen, T. Wu, A. Cohen, A. Gasparrini and H. Kan, Ambient Particulate Air Pollution And Daily Mortality In 652 Cities, N. Engl. J. Med., 2019, 381(8), 705-715.
- 5 B. Maher, I. Ahmed, V. Karloukovski, D. MacLaren, P. Foulds, D. Allsop, D. Mann, R. Torres-Jardón and Calderon-Garciduenas, Pollution Magnetite Nanoparticles In The Human Brain, Proc. Natl. Acad. Sci. U. S. A., 2016, 113(39), 10797-10801.
- 6 T. Wang, E. Chiang, L. Moreno-Vinasco, G. Lang, S. Pendyala, J. Samet, A. Geyh, P. Breysse, S. Chillrud, V. Natarajan and J. Garcia, Particulate Matter Disrupts Human Lung Endothelial Barrier Integrity Via ROS- And P38 MAPK-Dependent Pathways, Am. J. Respir. Cell Mol. Biol., 2010, 42(4), 442-449.
- 7 F. Schaumann, P. Borm, A. Herbrich, J. Knoch, M. Pitz, R. Schins, B. Luettig, J. Hohlfeld, J. Heinrich and N. Krug, Metal-Rich Ambient Particles (Particulate Matter 2.5) Cause Airway Inflammation In Healthy Subjects, Am. J. Respir. Crit. Care Med., 2004, 170(8), 898-903.
- 8 L. Wood, P. Gibson and M. Garg, Biomarkers Of Lipid Peroxidation, Airway Inflammation And Asthma, Eur. Respir. J., 2003, 21(1), 177-186.
- 9 N. Li, C. Sioutas, A. Cho, D. Schmitz, C. Misra, J. Sempf, M. Wang, T. Oberley, J. Froines and A. Nel, Ultrafine Particulate Pollutants Induce Oxidative Stress And Mitochondrial Damage, Environ. Health Perspect., 2003, **111**(4), 455–460.
- 10 A. Cho, C. Sioutas, A. Miguel, Y. Kumagai, D. Schmitz, M. Singh, A. Eiguren-Fernandez and J. Froines, Redox Activity Of Airborne Particulate Matter At Different Sites In The Los Angeles Basin, Environ. Res., 2005, 99(1), 40-47.
- 11 N. Janssen, A. Yang, M. Strak, M. Steenhof, B. Hellack, M. Gerlofs-Nijland, T. Kuhlbusch, F. Kelly, R. Harrison, B. Brunekreef, G. Hoek and F. Cassee, Oxidative Potential Of Particulate Matter Collected At Sites With Different Source Characteristics, Sci. Total Environ., 2014, 472, 572-581.
- 12 M. Strak, N. Janssen, K. Godri, I. Gosens, I. Mudway, F. Cassee, E. Lebret, F. Kelly, R. Harrison, B. Brunekreef, M. Steenhof and G. Hoek, Respiratory Health Effects Of Airborne Particulate Matter: The Role Of Particle Size, Composition, And Oxidative Potential—The RAPTES Project, Environ. Health Perspect., 2012, 120(8), 1183-1189.
- 13 A. Calas, G. Uzu, J. Martins, D. Voisin, L. Spadini, T. Lacroix and J. Jaffrezo, The Importance Of Simulated Lung Fluid (SLF) Extractions For A More Relevant Evaluation Of The Oxidative Potential Of Particulate Matter, Sci. Rep., 2017, 7(1), 1161.

- 14 A. Teja and P. Koh, Synthesis, Properties, And Applications Of Magnetic Iron Oxide Nanoparticles, Prog. Cryst. Growth Charact. Mater., 2009, 55(1-2), 22-45.
- 15 P. Nico, B. Kumfer, I. Kennedy and C. Anastasio, Redox Dynamics Of Mixed Metal (Mn, Cr, And Fe) Ultrafine Particles, Aerosol Sci. Technol., 2009, 43(1), 60-70.
- 16 C. Hennigan, A. Mucci and B. Reed, Trends In PM 2.5 Transition Metals In Urban Areas Across The United States, Environ. Res. Lett., 2019, 14(10), 104006.
- 17 E. Vidrio, H. Jung and C. Anastasio, Generation Of Hydroxyl Radicals From Dissolved Transition Metals In Surrogate Lung Fluid Solutions, Atmos. Environ., 2008, 42(18), 4369-4379.
- 18 B. Venkataramani, K. Venkateswarlu and J. Shankar, Sorption Properties Of Oxides, I. Colloid Interface Sci., 1978, 67(2), 187-194.
- 19 B. Dempsey and P. Singer, The Effect Of Calcium On The Adsorption Of Zinc By Mnox (S) And Fe(OH)3 (Am), J. Colloid Interface Sci., 1980, 79, 209-221.
- 20 D. Dzombak and F. Morel, Surface complexation modeling, Wiley, New York, 1990.
- 21 L. Chen and M. Lippmann, Effects Of Metals Within Ambient Air Particulate Matter (PM) On Human Health, Inhalation Toxicol., 2009, 21(1), 1-31.
- 22 J. Mirowsky, C. Hickey, L. Horton, M. Blaustein, K. Galdanes, R. Peltier, S. Chillrud, L. Chen, J. Ross, A. Nadas, M. Lippmann and T. Gordon, The Effect Of Particle Size, Location And Season On The Toxicity Of Urban And Rural Particulate Matter, Inhalation Toxicol., 2013, 25(13), 747-757.
- 23 J. Charrier and C. Anastasio, On Dithiothreitol (DTT) As A Measure Of Oxidative Potential For Ambient Particles: Evidence For The Importance Of Soluble Transition Metals, Atmos. Chem. Phys., 2012, 12(19), 9321-9333.
- 24 Y. Fujitani, A. Furuyama, K. Tanabe and S. Hirano, Comparison Of Oxidative Abilities Of PM 2.5 Collected At Traffic And Residential Sites In Japan. Contribution Of Transition Metals And Primary And Secondary Aerosols, Aerosol Air Qual. Res., 2017, 17(2), 574-587.
- 25 E. Software, MINEQL+ Chemical Equilibrium Modeling System, https://minegl.com/.
- 26 M. Lin and J. Yu, Dithiothreitol (DTT) Concentration Effect And Its Implications On The Applicability Of DTT Assay To Evaluate The Oxidative Potential Of Atmospheric Aerosol Samples, Environ. Pollut., 2019, 251(0269-7491), 938-944.
- Chemistry WebBook, https://webbook.nist.gov/ chemistry/, accessed Apr 18, 2020.
- 28 USA H, DR/890 Portable Colorimeter, Hach USA Downloads https://www.hach.com/dr-890-portablecolorimeter/product-downloads?id=7640439041.
- 29 D. Barthelmy, *Bixbyite Mineral Data*, http://webmineral.com/ data/Bixbyite.shtml#.XpmuMpl7lPY.
- 30 V. Verma, T. Fang, H. Guo, L. King, J. Bates, R. Peltier, E. Edgerton, A. Russell and R. Weber, Reactive Oxygen Species Associated With Water-Soluble PM_{2.5} In The Southeastern United States: Spatiotemporal Trends And Source Apportionment, Atmos. Chem. Phys., 2014, 14(23), 12915-12930.

- 31 P. Hsu, Crystallization Of Iron(III) Phosphate At Room Temperature, Soil Sci. Soc. Am. J., 1982, 46(5), 928-932.
- 32 A. Senn, R. Kaegi, S. Hug, J. Hering, S. Mangold and A. Voegelin, Composition And Structure Of Fe(III)-Precipitates Formed By Fe(II) Oxidation In Water At Near-Neutral Ph: Interdependent Effects Of Phosphate, Silicate And Ca, Geochim. Cosmochim. Acta, 2015, 162, 220-246.
- 33 B. Singh and M. Gräfe, Synchrotron-based techniques in soils and sediments, Elsevier, 2010.
- 34 L. Madsen and C. Koch, Kinetics Of Solution Crystal Growth Of Strengite, FePo₄ 2H₂O, J. Cryst. Growth, 2018, 482, 9-14.
- 35 J. Morgan and W. Stumm, Aquatic chemistry, Wiley, New York, 1981.
- 36 T. Grundl and J. Delwiche, Kinetics Of Ferric Oxyhydroxide Precipitation, *I. Contam. Hydrol.*, 1993, **14**(1), 71–87.
- 37 M. Schoonen, C. Cohn, E. Roemer, R. Laffers, S. Simon and T. O'Riordan, Mineral-Induced Formation Of Reactive Oxygen Species, Rev. Mineral. Geochem., 2006, 64(1), 179-2.2.1
- 38 W. Sung and J. Morgan, Kinetics And Product Of Ferrous Iron Oxygenation In Aqueous Systems, Environ. Sci. Technol., 1980, 14(5), 561-568.
- 39 S. Faust and O. Aly, Chemistry of Water Treatment, Taylor & Francis, 2nd edn, 1998.
- 40 T. Angele Ngantcha-Kwimi and B. Reed, As(V) And PO₄ Removal By An Iron-Impregnated Activated Carbon In A Single And Binary Adsorbate System: Experimental And Surface Complexation Modeling Results, J. Environ. Eng., 2016, 142(1), 04015046.

- 41 E. DiStefano, A. Eiguren-Fernandez, R. Delfino, C. Sioutas, J. Froines and A. Cho, Determination Of Metal-Based Hydroxyl Radical Generating Capacity Of Ambient And Diesel Exhaust Particles, Inhalation Toxicol., 2009, 21(9),
- 42 P. Lakey, T. Berkemeier, H. Tong, A. Arangio, K. Lucas, U. Pöschl and M. Shiraiwa, Chemical Exposure-Response Relationship Between Air Pollutants And Reactive Oxygen Species In The Human Respiratory Tract, Sci. Rep., 2016, 6(1), 32916.
- 43 U. Kodavanti, R. Hauser, D. Christiani, Z. Meng, J. McGee, A. Ledbetter, J. Richards and D. Costa, Pulmonary Responses To Oil Fly Ash Particles In The Rat Differ By Virtue Of Their Specific Soluble Metals, Toxicol. Sci., 1998, 43(2), 204-212.
- 44 M. Bell, K. Ebisu, R. Peng, J. Samet and F. Dominici, Hospital Admissions And Chemical Composition Of Fine Particle Air Pollution, Am. J. Respir. Crit. Care Med., 2009, 179(12), 1115-1120.
- 45 B. Ostro, W. Feng, R. Broadwin, S. Green and M. Lipsett, The Effects Of Components Of Fine Particulate Air Pollution On Mortality In California: Results From CALFINE, Environ. Health Perspect., 2007, 115(1), 13-19.
- 46 D. Gonzalez, C. Cala, Q. Peng and S. Paulson, HULIS Enhancement Of Hydroxyl Radical Formation From Fe(II): Kinetics Of Fulvic Acid-Fe(II) Complexes In The Presence Of Lung Antioxidants, Environ. Sci. Technol., 2017, 51(13), 7676-7685.